264 KSME Journal, Vol. 8, No. 3, pp. 264~276, 1994

Numerical Solution of Two-Dimensional or Axi-Symmetric Incompressible Flow Using the Vorticity Equations

Yang-Moon Koh* and P. Bradshaw**

(Received November 19, 1993)

A method to integrate the vorticity-velocity form of two-dimensional or axi-symmetric incompressible Navier-Stokes equations is described. The method employs equi-potential lines and streamlines of an inviscid flow as coordinate lines and the velocity field is determined from the vorticity distribution with boundary conditions on the normal velocity only, while the tangential velocities are used as boundary conditions for the vorticity. The results of numerical experiments on time-dependent flow past an impulsively started circular cylinder and sphere are, then, presented to demonstrate the performance of the scheme. Numerical results show that the present method is very stable and accurate.

Key Words: Incompressible Flow, Velocity-Vorticity Formulation, Equi-Potential and Streamline Coordinates, Circular Cylinder, Sphere.

Nomenclature

English symbols

a : Radius of a circular cylinder
C_D : Drag coefficient
h_ϕ, h_ψ, h_3 : Scale factors of $\phi-\psi$ coordinate system
L : Reference length
m : Flow index, 0 in two-dimensional flow and 1 in axi-symmetric flow
p, p_t : Static and total pressure
q_p : Potential flow speed, $(v_x^2+v_y^2)^{1/2}$
Re : Reynolds number, U_0L/ν
Q_ϕ, Q_ψ : Components of vorticity flux
$\boldsymbol{Q}$: Vorticity flux vector, Eq. (5)
t : Time
u : ϕ-component of velocity
U_o : Reference velocity
v : ψ-component of velocity
v_x, v_y : Velocity components of potential flow
$\boldsymbol{v}$: Velocity vector
x, y : Cartesian or axi-symmetric cylindrical coordinates

Greek symbols

α, β : Stability parameters, Eqs. (44) and (45)
δ_τ, δ_ϕ, δ_ψ : Differencing operators, Eq. (28)
$\Delta\tau$, $\Delta\phi$, $\Delta\psi$: Incremental changes in τ, ϕ and ψ
Δn_{min} : Minimum distance between adjacent ψ-lines
$\Delta\psi_{min}$: Minimum of $\Delta\psi=\psi_{j+1}-\psi_j$
μ_τ, μ_ϕ, μ_ψ : Averaging operators, Eq. (29)
μ : Viscosity
ν : Kinematic viscosity
ρ : Density
τ : Dimensionless time, U_0t/L
ϕ : Velocity potential
ϕ_f, ϕ_b : Velocity potentials at stagnation points, Fig. 1(b)
ϕ_s, ϕ_e : Limits of computational region in ϕ-direction, Fig. 1(b)
ψ : Stream function
ψ_e : Limit of computational region in ψ-direction, Fig. 1(b)
ω, $\boldsymbol{\omega}$: Vorticity

*Department of Mechanical Engineering, University of Ulsan, Ulsan 680-749, South Korea
**Department of Mechanical Engineering, Stanford University, Stanford CA94305, USA

1. Introduction

The incompressible Navier-Stokes equations are much simpler than the compressible ones, but look more difficult to solve numerically. The absence of time derivative in the continuity equation makes it hard to provide an appropriate time-marching procedure. Another cause of the computational difficulty is that the continuity equation contains only velocity components, and there is no obvious link with pressure as there is for compressible flow through the density (Fletcher, 1988, p. 328). These difficulties are usually worked out by employing the Poisson equation for pressure instead of the continuity equation (Harlow and Welch, 1965; Chorin, 1968; Patankar and Spalding, 1972) or, in two dimensions, by introducing the stream function (Campion-Renson and Crochet, 1978; Rubin and Khosla, 1981; Jordan, 1992).

The vorticity-velocity formulation can be another alternate approach to the numerical solution of the incompressible Navier-Stokes equations. The kinematic definition of vorticity together with the continuity equation can be used to get the velocity field, while the vorticity distribution is got from the vorticity transport equation. In previous studies (Fasel, 1976 ; Dennis et al., 1979 ; Fasel and Booz, 1984; Bontoux et al., 1986), the velocity field was usually obtained by solving the Poisson equation

$$\nabla^2 \boldsymbol{v} = -\nabla \times \boldsymbol{\omega}. \tag{1}$$

Gatski et al.(1982; 1989), on the other hand, got the velocity field directly from the discrete form of the continuity equation and the kinematic definition of vorticity. Koh(1987) showed that the resulting system of algebraic equations got by discretizing the definition of vorticity and continuity eqaution can be reduced to a more easily tractable system of equations, and one needs to solve, in effect, only one three-dimensional and then one two-dimensional Poisson equation to get all the three velocity components.

In curvilinear coordinates, however, Eq. (1) does not decompose into three Poisson equations for each of the velocity components and it becomes difficult to solve it. Likewise, Koh's method(Koh, 1987) is applicable to the equations expressed in rectangular Cartesian coordinates only. It means that the method will be difficult to be used to solve the problems with curved boundaries. This paper treats the velocity-vorticity formulation for the unsteady two-dimensional or axi-symmetric incompressible flows and a method to solve them, which can be used to solve any two-dimensional or axi-symmetric incompressible flow problems. Equi-potential lines and streamlines of an inviscid flow are used as coordinate lines and the geometric complexity has virtually no effect on the solving procedure. One needs only to solve the potential flow in addition. Then the remaining numerical procedures will be nearly the same in all cases and can be done in routine. Though only two-dimensional and axi-symmetric flows are considered here, the present method can also be extended easily to three-dimensional flows over two-dimensional or axi-symmetric bodies, e.g., flows over yawed cylinders and bodies of revolution.

In the remainder of this paper, the method will be described in detail and demonstrated via sample examples, the time-dependent flow past an impulsively started circular cylinder and sphere. Numerical results show that the present method is very stable and accurate.

2. Governing Equations and Boundary Conditions

2.1 Governing equations

The continuity equation,

$$\nabla \cdot \boldsymbol{v} = 0, \tag{2}$$

definition of vorticity,

$$\nabla \times \boldsymbol{v} = \boldsymbol{\omega}, \tag{3}$$

and vorticity transport equation,

$$\frac{\partial \boldsymbol{\omega}}{\partial \tau} = \nabla \times \boldsymbol{Q}, \tag{4}$$

together with

$$\boldsymbol{Q}=\boldsymbol{v}\times\boldsymbol{\omega}-\frac{1}{Re}\nabla\times\boldsymbol{\omega}, \tag{5}$$

form a complete system of equations for the incompressible flow and the velocity $\boldsymbol{v}$ and vorticity $\boldsymbol{\omega}$ can be obtained by solving the above system of equations with appropriate boundary conditions. The pressure p can then be calculated from the momentum equation,

$$-\nabla\left(p+\frac{1}{2}\boldsymbol{v}\cdot\boldsymbol{v}\right)=\frac{\partial\boldsymbol{v}}{\partial\tau}-\boldsymbol{Q}, \tag{6}$$

which is, in fact, the integral of the vorticity transport equation, Eq. (4). In the above equations, all variables are non-dimensionalized using the reference velocity U_0 and reference length L. Thus the dimensionless time τ and Reynolds number Re become, respectively,

$$\tau=\frac{U_0 t}{L}$$

and

$$Re=\frac{U_0 L}{\nu},$$

where ν is the kinematic viscosity of the fluid.

2.2 Transformation of governing equations

In a two-dimensional or axi-symmetric potential flow the velocity potential ϕ and stream function (Stokes' stream function when the flow is axi-symmetric) ψ are related to the velocity components v_x, v_y by equations

$$d\phi=v_x dx+v_y dy \tag{7}$$

and

$$d\psi=-y^m v_y dx+y^m v_x dy, \tag{8}$$

where the exponent m is 0 for the two-dimensional flow and 1 for the axi-symmetric one. In the axi-symmetric flow x and y are the distance along and from the axis of symmetry, respectively. Thus the scale factos h_ϕ, h_ψ of the ϕ-ψ coordinate system become

$$h_\phi=\frac{1}{q_p} \tag{9}$$

and

$$h_\psi=\frac{1}{y^m q_p}, \tag{10}$$

where

$$q_p^2=v_x^2+v_y^2.$$

In addition, we need the third scale factor h_3 which becomes

$$h_3=y^m,$$

when, as the third coordinate, the distance normal to the $\phi-\psi$ plane is taken in a two-dimensional flow and the azimuthal angle in an axi-symmetric flow.

The complex flow region in the physical x-y space is transformed into a rectangular region $\{\phi_s<\phi<\phi_e,\ 0<\psi<\psi_e\}$ in the $\phi-\psi$ coordinate space (Fig. 1) and Eqs. (2) to (5) become, respectively,

$$q_p^2\left(\frac{\partial u/q_p}{\partial\phi}+\frac{\partial y^m v/q_p}{\partial\psi}\right)=0, \tag{11}$$

$$y^m q_p^2\left(\frac{\partial v/y^m q_p}{\partial\phi}-\frac{\partial u/q_p}{\partial\psi}\right)=\omega, \tag{12}$$

$$\frac{\partial\omega}{\partial\tau}=-y^m q_p^2\left(\frac{\partial Q_\phi/y^m q_p}{\partial\phi}+\frac{\partial Q_\psi/q_p}{\partial\psi}\right), \tag{13}$$

$$Q_\phi=u\omega-\frac{q_p}{Rey^m}\frac{\partial y^m\omega}{\partial\phi}, \tag{14}$$

and

$$Q_\psi=v\omega-\frac{q_p}{Re}\frac{\partial y^m\omega}{\partial\psi}, \tag{15}$$

where, u, v, and ω represent the velocity components in $\phi-$ and $\psi-$directions and vorticity, respectively.

To derive Eq. (13) from Eq. (4), one should

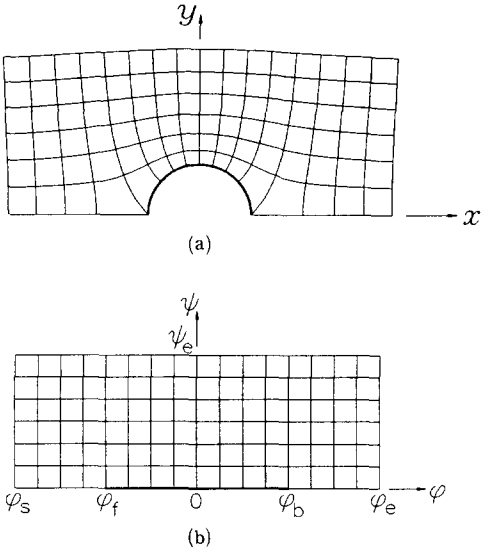

Fig. 1 Mapping of the flow region. (a) Physical x-y space; (b) Computational ϕ-ψ space

note that Q_ψ is not the ψ-component but the ϕ-component of the vector $\boldsymbol{Q}$. Similarly $-Q_\phi$ is the ψ-component of $\boldsymbol{Q}$. In a two-dimensional flow, Q_ϕ and Q_ψ defined as above can be interpreted as components of the vorticity-flux vector in ϕ- and ψ-directions, respectively. But, in a three-dimensional flow, the physical meaning of the vector $\boldsymbol{Q}$ is not clear. Truesdell (1954, p. 77) identified the convective part $\boldsymbol{v}\times\boldsymbol{\omega}$ of $\boldsymbol{Q}$ as a Lamb vector.

If we put

$$\begin{aligned} &u'=u/q_q, \qquad v'=v/q_p, \\ &Q'_\phi=Q_\phi/q_p, \text{ and } Q'_\psi=Q_\psi/q_p, \end{aligned} \tag{16}$$

Eqs. (11) to (15) are simplified, deleting primes from dependent variables, to

$$\frac{\partial u}{\partial\phi}+\frac{\partial y^m v}{\partial\psi}=0, \tag{17}$$

$$\frac{\partial v/y^m}{\partial\phi}-\frac{\partial u}{\partial\psi}=\frac{\omega}{y^m q_p^2}, \tag{18}$$

$$\frac{\partial\omega/y^m q_p^2}{\partial\tau}=-\frac{\partial Q_\phi/y^m}{\partial\phi}-\frac{\partial Q_\psi}{\partial\psi}, \tag{19}$$

$$Q_\phi=u\omega-\frac{1}{Rey^m}\frac{\partial y^m\omega}{\partial\phi}, \tag{20}$$

and

$$Q_\psi=v\omega-\frac{1}{Re}\frac{\partial y^m\omega}{\partial\psi}, \tag{21}$$

respectively. It is simple to decouple the velocity component v from u in Eqs. (17) and (18) and get

$$\frac{\partial^2 v/y^m}{\partial\phi^2}+\frac{\partial^2 y^m v}{\partial\psi^2}=\frac{\partial}{\partial\phi}\left(\frac{\omega}{y^m q_p^2}\right) \tag{22}$$

which may be used as the governing equation instead of Eq. (18). But, because of reasons explained in the next section, we will take Eq. (18) rather than Eq. (22) as the governing equation.

2.3 Boundary conditions

The motion of a (compressible) fluid occupying any limited simply-connected region is determinate when we know the values of the expansion, and of the component vorticities, at every point of the region, and the value of the normal velocity at every point of the boundary (Lamb, 1945, p. 207). Thus to get velocities inside the region from Eqs. (17) and (18) the normal components of velocities on boundaries are necessary. To compute vorticities in the region from Eq. (19) which is a parabolic partial differential equation, the value of the vorticity or its flux at the boundary must be known. Thus the appropriate boundary conditions to solve the system of governing equations are conditions on the normal velocity components and tangential vorticities at the boundary of the region.

In most practical problems, the boundary conditions are given in terms of velocities rather than vorticities. But this does not usually cause any difficulty. In most external flows, as an example, we can assume that vorticities will be zero at inflow boundaries and at boundaries far from the solid body and that the normal components of vorticity gradients will be zero at the outgoing boundary. On solid boundaries, however, some care should be taken. The condition on the normal velocity can be used with Eqs. (17) and (18) to determine the velocity in the region. But the velocity thus determined may not satisfy the no-slip condition, unless the vorticity distribution is such that the resulting velocity satisfies it. In other words the no-slip condition is not a condition for the velocity but for the vorticity. This is understandable, if we consider that the solid boudary is a *distributed source* of vorticity and that the vorticity is continuously generated at the solid boundary to make the relative velocity there zero (Lighthill, 1963, p. 54). Thus we have boundary conditions for the flow, say, around a symmetric body which is set impulsively to move in a constant velocity as (Fig. 1(b))

$$\begin{aligned} &u=1, \quad \omega=0 \quad \text{at } \phi=\phi_s, \\ &\frac{\partial u}{\partial\phi}=0, \quad \frac{\partial\omega}{\partial\phi}=0 \quad \text{at } \phi=\phi_e, \\ &v=0, \quad \omega=0 \quad \text{at} \begin{cases} \psi=0 \\ \phi<\phi_f,\ \phi>\phi_b \end{cases} \\ &v=0, \quad \omega=0 \quad \text{at } \psi=\psi_e, \\ &u=0, \quad v=0 \quad \text{at} \begin{cases} \psi=0 \\ \phi_f<\phi<\phi_b \end{cases} \end{aligned} \tag{23}$$

where ϕ_f and ϕ_b are velocity potentials at the front and rear stagnation point, respectively. In certain cases (say, the internal flow or the uniform shear flow), inflow vorticities are not zero and should be specified accordingly (and normal velocities as well).

2.4 Equations for pressure

Once the velocity and vorticity are determined, the pressure can be obtained by integrating the momentum equation, Eq. (6), or

$$-\frac{\partial p_t}{\partial \phi}=\frac{\partial u}{\partial \tau}-Q_\psi \tag{24}$$

and

$$-y^m\frac{\partial p_t}{\partial \psi}=\frac{\partial v}{\partial \tau}+Q_\phi, \tag{25}$$

where p_t is a total pressure, i.e.,

$$p_t=p+\frac{1}{2}(u^2+v^2)\,q_p^2. \tag{26}$$

To compute the pressure at a point, integration can be done following any paths connected by lines of constant ϕ's and ψ's from a point of reference to that point. Equation (6) says that the vector $\partial \boldsymbol{v}/\partial\tau-\boldsymbol{Q}$ is irrotational and, thus, its integral does not depend on the path integration.

3. Numerical Procedures

3.1 Computational grid system and discretization

The computational grid system used in the present work is shown in Fig. 2 together with the locations of the variables on the cell. The computational domain is subdivided into computational cells by grid lines,

$$\phi=\phi_i,\quad i=0,1,2,\cdots,\ i_{max},$$

and

$$\psi=\psi_j,\quad j=0,1,2,\cdots,j_{max}.$$

Let

$$\Delta\phi_{i+1/2}=\phi_{i+1}-\phi_i$$

and

$$\Delta\psi_{j+1/2}=\psi_{j+1}-\psi_j.$$

In addition, we draw auxiliary grid lines,

$$\phi_{i+1/2}=\frac{\phi_{i+1}+\phi_i}{2},\quad \psi_{j+1/2}=\frac{\psi_{j+1}+\psi_j}{2},$$

and

$$\Delta\phi_i=\phi_{i+1/2}-\phi_{i-1/2},\quad \Delta\psi_j=\psi_{j+1/2}-\psi_{j-1/2}.$$

We will also write

$$f^k_{i,j+1/2}=f(\phi_i,\psi_{j+1/2},\ k\Delta\tau) \tag{27}$$

etc., where f represents any dependent variable and $\Delta\tau$ a time step, and employ the notation

$$\begin{aligned}\delta_\phi f^k_{i,j}&=(f^k_{i+1/2,j}-f^k_{i-1/2,j})/\Delta\phi_i,\\ \delta_\psi f^k_{i,j+1/2}&=(f^k_{i,j+1}-f^k_{i,j})/\Delta\psi_{j+1/2},\\ \delta_\tau f^{k+1/2}_{i,j}&=(f^{k+1}_{i,j}-f^k_{i,j})/\Delta\tau,\end{aligned} \tag{28}$$

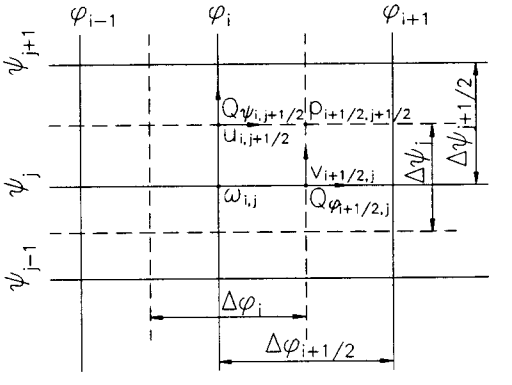

(a) Internal mesh

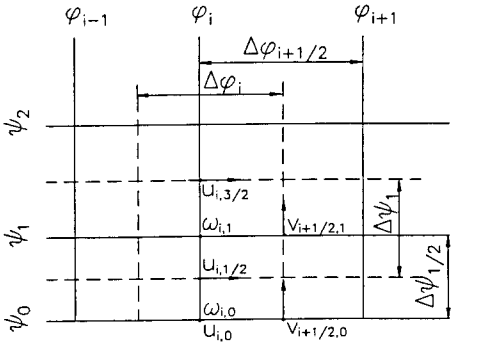

(b) Mesh near the boundary $\psi=0$

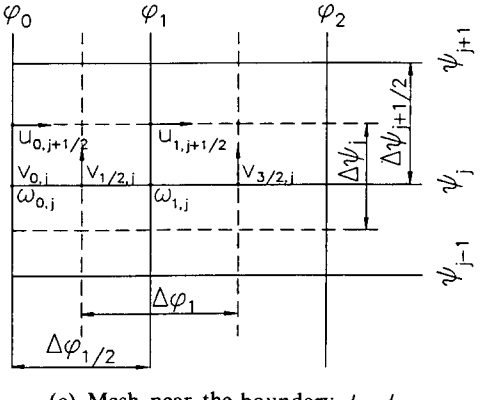

(c) Mesh near the boundary $\phi=\phi_s$

Fig. 2 Staggered mesh

and

$$\mu_\phi f^k_{i,j}=(f^k_{i+1/2,j}+f^k_{i-1/2,j})/2,$$
$$\mu_\phi f^k_{i,j+1/2}=(f^k_{i,j+1}+f^k_{i,j})/2,$$
$$\mu_\tau f^{k+1/2}_{i,j}=(f^{k+1}_{i,j}+f^k_{i,j})/2. \tag{29}$$

The vorticity $\omega_{i,j}$ and pressure $p_{i+1/2,j+1/2}$ are to be interpreted as averages over the corresponding cells, $\{\phi_{i-1/2}<\phi<\phi_{i+1/2},\ \psi_{j-1/2},\ \psi<\psi<_{j+1/2}\}$ and $\{\phi_i<\phi<\phi_{i+1},\ \psi_j<\psi<\psi_{j+1}\}$, respectively, and velocities and vorticity fluxes as averages over the sides of the cell. Then Eqs. (17), (18) and (19) are discretized as

$$\delta_\phi u^{k+1}_{i+1/2,j+1/2}+\delta_\psi(y^m v)^{k+1}_{i+1/2,j+1/2}=0, \tag{30}$$
$$\delta_\phi(v/y^m)^{k+1}_{i,j}-\delta_\psi u^{k+1}_{i,j}=(\omega/y^m q_p^2)^{k+1}_{i,j}, \tag{31}$$

and

$$\delta_\tau(\omega/y^m q_p^2)^{k+1/2}_{i,j}$$
$$=-\delta_\phi(Q_\phi/y^m)^{k+1/2}_{i,j}-\delta_\psi Q_{\psi i,j}^{k+1/2} \tag{32}$$

Q_ϕ and Q_ψ are defined at the v- and u-points, respectively, and so the velocity components u, v in Eqs. (20) and (21) should be represented by the averages of corresponding velocity components at neighbouring four points. In addition, we discretize the convective and diffusive terms of Eqs. (20) and (21) using the explicit upwind differencing and implicit Crank-Nicolson scheme, respectively. Thus we have

$$Q^{k+1/2}_{\phi i+1/2,j}=\mu_\phi\mu_\psi u^k_{i+1/2,j}\omega^k_{i+1/2\pm1/2,j}$$
$$-\frac{1}{Re\,(y_{i+1/2,j})^m}\mu_\tau\delta_\phi(y^m\omega)^{k+1/2}_{i+1/2,j} \tag{33}$$

and

$$Q^{k+1/2}_{\psi i,j+1/2}=\mu_\phi\mu_\psi v^k_{i+1/2,j}\omega^k_{i+1/2\mp1/2,j}$$
$$-\frac{1}{Re_{(y_{i+1/2,j})}}\mu_\tau\delta_\psi(y^m\omega)^{k+1/2}_{i+1/2,j} \tag{34}$$

where the minus must be taken from the $\mp$ sign, when the average velocity $\mu_\phi\mu_\psi u$ or $\mu_\phi\mu_\psi v$ is positive.

Implementation of boundary conditions (23) is straightforward but at the solid and outgoing boundary. For nodes on the solid boundary (Fig. 2(b)), Eq. (31) is modified to

$$\delta_\phi\left(\frac{v}{y^m}\right)^{k+1}_{i,0}-\frac{u^{k+1}_{i,1/2}-u^{k+1}_{i,0}}{\Delta\psi_{1/2}/2}$$
$$=\left(\frac{\omega}{y^m q_p^2}\right)^{k+1}_{i,0}, \tag{35}$$

from which the vorticity $\omega^{k+1}_{i,0}$ at the solid boundary can be computed. Note that, on the boundary, there are points for vorticities and normal velocities only, and the tangential velocity $u_{i,0}$ is defined at the vorticity point and used to get the tangential vorticity $\omega_{i,0}$.

For nodes on the outflow boundary, rather than trying to implement the Neumann condition

$$\frac{\partial u}{\partial\phi}=\frac{\partial\omega}{\partial\phi}=0$$

directly, we have adopted the simpler procedure. The continuity equation, Eq. (17), together with the above Neumann condition, gives

$$-\frac{\partial y^m v}{\partial\psi}=0$$

and, hence,

$$v=0 \quad \text{at} \quad \phi=\phi_e.$$

Thus we can put

$$v^{k+1}_{imax-1/2,j}=0.$$

For the vortivity, we simply put

$$\omega^{k+1}_{imax,j}=\omega^{k+1}_{imax-1,j}.$$

3.2 Solution procedure

The system of algebraic equations consisting of Eqs. (30) to (35) and those derived from boundary conditions will form the complete system of equations for the variables, u^{k+1}'s, v^{k+1}'s, and ω^{k+1}'s. Instead of trying to get the exact solution of this complicated system of equations for the flow field at $t=(k+1)\Delta\tau$, we have tried to get an approximate solution as follows. Noting that vorticities ω^{k+1}'s are coupled to velocities u^{k+1}'s and v^{k+1}'s only through boundary conditions such as Eq. (35), they are decoupled by assuming that the vorticity is not generated continuously but spontaneously only at the end of the interval $\Delta\tau$. In other words, on the solid boundary the normal vorticity flux Q_ψ is assumed zero during the whole interval $\Delta\tau$ except just at the end of the interval. Thus we have vorticity transport equations for nodes on the solid boundary as

$$\delta_\tau(\omega/y^m q_p^2)^{k+1/2}_{i,0}$$
$$=-\delta_\phi(Q_\phi/y^m)^{k+1/2}_{i,0}-2Q^{k+1/2}_{\psi i,1/2}/\Delta\psi_{1/2} \tag{36}$$

which will, together with those for internal nodes, form the complete system for ω^{k+1}'s. Now ω^{k+1}'s can be solved easily, as the resulting system of algebraic equations is diagonal-dominant. Then

velocities are computed from Eqs. (30) and (31) with conditions on the normal velocity at the boundary (the explanation of the method follows) and, finally, the vorticities at the solid boundary are adjusted using Eq. (35) so that the no-slip condition is satisfied.

In brief, the numerical procedure is composed of three steps. In *Step 1* the vorticity field in the region is computed implicitly assuming that the vorticity flux from the solid wall is zero. In *Step 2* the velocity field is solved from the vorticity field obtained at *Step 1* and boundary conditions on the normal velocity only. Finally, in *Step 3* vorticities at the solid boundary are adjusted so that the no-slip condition is satisfied.

An efficient method to compute the three-dimensional velocity field from the continuity equation and definition of vorticity in a rectangular Cartesian coordinate system is suggested by Koh(1987) and is adopted in the present work. The method is to decouple velocity components in each direction from the others and solve them one by one; for the axi-symmetric flow only v's can be decoupled from u's. Since δ_ϕ and δ_ψ are commutable, i.e.,

$$\delta_\psi\delta_\phi u_{i+1/2,j}=\delta_\phi\delta_\psi u_{i+1/2,j},$$

we have fron Eqs. (30) and (31)

$$\delta_\phi\delta_\phi(v/y^m)^{k+1}_{i+1/2,j}+\delta_\phi\delta_\psi(y^m v)^{k+1}_{i+1/2,j} =\delta_\phi(\omega/y^m q_p^2)^{k+1}_{i+1/2,j}, \tag{37}$$

for internal nodes, i.e., for

$$i=1,2,\cdots,\ i_{max}-2,$$

and

$$j=1,2,\cdots,j_{max}-1.$$

Eq. (37) is not applicable to velocities such as $v^{k+1}_{1/2,j}$'s adjacent to the boundary $\phi=\phi_S$, since $v_{-1/2,j}$'s are at the outside of the domain and not defined. Instead we can get the modified equation as follows (Fig. 2(c)). For nodes adjacent to the boundary $\phi=\phi_s$, Eq. (30) becomes

$$\frac{u^{k+1}_{1,j+1/2}-u^{k+1}_{0,j+1/2}}{\Delta\phi_{1/2}}+\delta_\psi(y^m v)^{k+1}_{1/2,j+1/2}=0,$$

or, operating with the difference operator δ_ψ,

$$\frac{\delta_\psi u^{k+1}_{1,j}}{\Delta\phi_{1/2}} =\frac{\delta_\psi u^{k+1}_{0,j}}{\Delta\phi_{1/2}}-\delta_\psi\delta_\psi(y^m v)^{k+1}_{1/2,j}. \tag{38}$$

Thus, by substituting $\delta_\psi u^{k+1}_{1,j}$ by Eq. (38), we have from Eq. (31)

$$\frac{\delta_\phi(v/y^m)^{k+1}_{1,j}}{\Delta\phi_{1/2}}+\delta_\psi\delta_\psi(y^m v)^{k+1}_{1/2,j} =\frac{1}{\Delta\phi_{1/2}}\left[\left(\frac{\omega}{y^m q_p^2}\right)^{k+1}_{1,j}+\delta_\psi u^{k+1}_{0,j}\right] \tag{39}$$

Eqs. (37) and (39) form the complete system of equations for v^{k+1}'s and can be solved without difficulty using, say, the successive-over-relaxation method. Once v^{k+1}'s are obtained, u^{k+1}'s can be got from the continuity equaion, Eq. (30).

Equation (37) can be got directly from Eq. (22) as usual, but, if we had started from this elliptic equation, it might not have been so simple to get Eq. (39) and we should have had recourse to the tangential velocity at the boundary again to get the velocity field in the region. Another point to be noted is that Eq. (22) is not obtained just by taking the curl of the vorticity-defining equation, Eq. (12), but from Eq. (18) which is the vorticity-defining equation divided by $y^m q_p^2$. The vector equation

$$\nabla^2\boldsymbol{v}=-\nabla\times\boldsymbol{\omega} \tag{40}$$

decomposes into three scalar equations like

$$\nabla^2 u=-\frac{\partial\omega_z}{\partial y}+\frac{\partial\omega_y}{\partial z}$$

only when it is expressed in Cartesian coordinates. Decoupling of v's from u's in Eqs. (11) and (12) would have been hard to spot, if the Poisson equation, Eq. (40), had used as the governing equation.[1)]

Finally, we have, from Eqs. (24) and (25),

$$-\delta_\phi p_t{}^{k+1}_{i,j+1/2}=\delta_\tau u^{k+1}_{i,j+1/2}-Q_\phi{}^{k+1}_{i,j+1/2} \tag{41}$$

and

$$-(y_{i+1/2,j})^m\delta_\psi p_t{}^{k+1}_{i+1/2,j} =\delta_\tau v^{k+1}_{i+1/2,j}+Q_\phi{}^{k+1}_{i+1/2,j}. \tag{42}$$

1) It is not difficult to show that a similar procedure to compute velocity components in each direction, one by one, can be applied also when the equations are expressed in cylindrical or spherical coordinates.

Eqs. (41) and (42) are not at $\tau=(k+1/2)\Delta\tau$ but at $(k+1)\Delta\tau$. It is found that the computed values of unsteady pressure, especially contributions from the term $\partial v/\phi\tau$, are rather sensitive to the time-advancing scheme and that it gives better results when the same time-advancing scheme is used for each term. Thus, rather than computing the pressure $p^{k+1/2}$ at $\tau=(k+1/2)\Delta\tau$ using those values already obtained such as $\delta_\tau u^{k+1/2}$'s and $Q_\phi^{k+1/2}$'s, we compute the pressure p^{k+1} at $\tau=(k+1)\Delta\tau$ from values of velocities and vorticities at $\tau=(k+1)\Delta\tau$ using the explicit Euler method.

4. Test Calculations and Results

The time-dependent flow past an impulsively started circular cylinder at Reynolds numbers, based on the radius a of the cylinder and oncoming velocity U_0, of 1, 10, and 4500 has been computed. We selected this 'classic' example because exact analytical results of boundary-layer approximation is availiable for small $\tau(=U_0t/a<<1$, where t is the time elapsed since the start of motion) (Koh, 1993a).

To cover the wide range of Reynolds numbers and also to check the grid-dependency of the method, four different grids are used for the simulation of the flow around the circular cylinder. Figure 3 shows one of them (*Grid 1*). The number of grid lines in *Grid 1* is 71 in the ϕ-direction and 36 in the ψ-direction. 31 ϕ-lines meet the upper surface of the cylinder at 6 degree intervals and, then, the meshes are increased uniformly on both sides of the cylinder, but restricted to half of the radius. $\Delta\psi$'s are also taken very small near the body and increased in geometric progression but to 0.5 again. Other grids are basically same as *Grid 1* but different in details such as the number of grid lines, the minimum and maximum spacing, etc. Important parameters of the grids used for the computation of the flow around the circular cylinder are in Table 1.

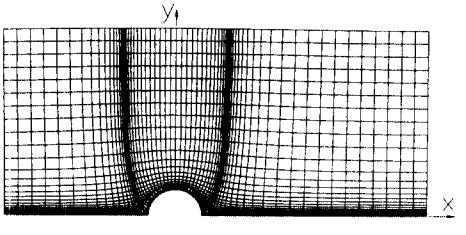

Fig. 3 Computational grid for a circular cylinder (*Grid 1*)

The drag coefficients C_D at $Re=1$ and 10 calculated using *Grid 1* and *3* are plotted in Fig. 4(a) and (b), respectively, together with the analytical result(Koh, 1993a),

$$ReC_D=4\sqrt{\pi}\left[\left(\frac{\tau}{Re}\right)^{-0.5}+1\right],\quad \tau/Re<<1. \tag{43}$$

Fig. 4(a) shows that the agreement between our computed values and analytic ones is quite good up to $\tau/Re\approx0.01$. Figure 4(b), however, shows that the numerical results computed using *Grid 3* deviate slightly from the analytic ones at very small time, say, at $\tau/Re\approx10^{-4}$. This is because the boundary layer at this small time is too thin to be resolved by *Grid 3* (Table 1). Two computed values of the drag coefficient at the same Reynolds number are different one another at $\tau/Re\approx1$ again; values computed from *Grid 1* (Fig. 4(a)) are larger than those from *Crid 3* (Fig. 4(b)). This seems due to the blockage or "displacement" effect.

Behaviour of the computed drag coefficients with respect to time τ is shown in Fig. 5. All the drag coefficients shown in the figure are at $Re=4500$ and calculated using the same grid (*Grid 4*) but with different time intervals $\Delta\tau$. The singular

Table 1 Grids for the flow around a circular cylinder

	Grid 1	*Grid 2*	*Grid 3*	*Grid 4*
ϕ_s	-6.56	-6.56	-11.71	-6.56
ϕ_e	9.56	9.56	17.71	19.56
ψ_e	7.11	7.17	18.42	11.0
Grid Lines	71×36	71×36	71×36	91×51
$\Delta\phi_{min}$	0.0110	0.0110	0.0110	0.0110
$\Delta\phi_{max}$	0.5	0.5	1.0	0.5
$\Delta\psi_{min}$	0.002	0.001	0.02	0.0004
$\Delta\psi_{max}$	0.5	0.5	1.0	0.5

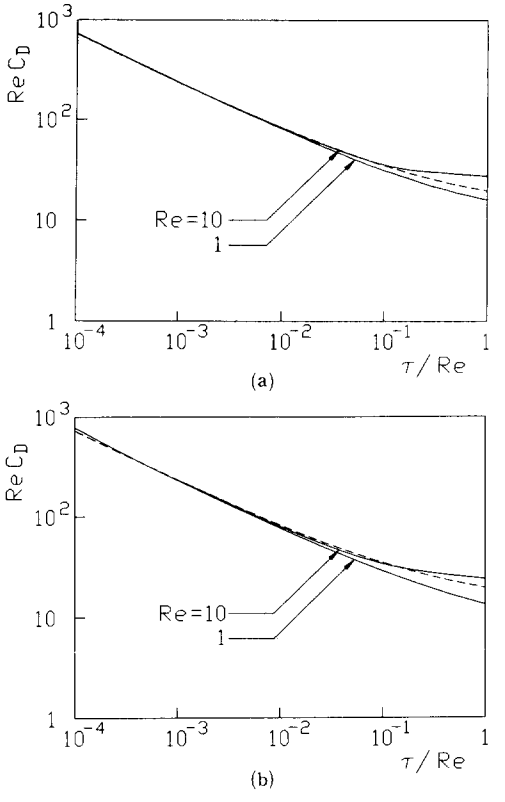

Fig. 4 Drag coefficient of an impulsively started circular cylinder computed using two different grids. (a) *Grid 1*; (b) *Grid 3*. ——, Present results; - - -, Analytic resuts, Eq. (43)

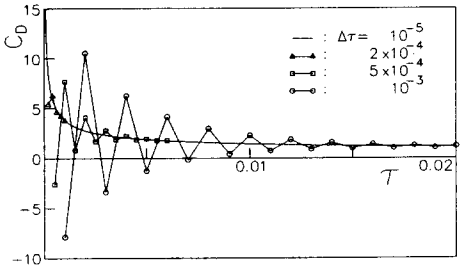

Fig. 5 Drag coefficients of an impulsively started circular cylinder computed using various time-step sizes ($Re=4500$, *Grid 4*)

initial condition makes the computed drag (and the flow field as well) fluctuate for a while, but the fluctuation dampens quickly and the numerical procedure is stabilized. Though not shown in the figure, we have found that the procedure is still stable with $\Delta\tau=0.01$. With this large $\Delta\tau$, however, it takes a rather long time, about 500 time-steps, for the fluctuation to die out sufficiently.

The stability and accuracy of the numerical method depend not on $\Delta\tau$ but on the ratio of it to the convection and/or diffusion time across the computational cell. Thus, considering that the convection is mainly along the streamline and the diffusion normal to the solid surface, we can define two parameters, α and β, such as

$$\alpha=\frac{\Delta\tau}{\Delta\phi_{min}} \tag{44}$$

and

$$\beta=\frac{4\Delta\tau}{Re(\Delta\phi_{min})^2}. \tag{45}$$

The parameter α is, in fact, the Courant number, and the factor 4 in the definition of the parameter β is because the minimum physical spacing Δn_{min} between two grid lines, $\psi=\psi_0(=0)$ and $\psi=\psi_1$, adjacent to the wall is half of $\Delta\psi_{min}=\psi_1-\psi_0$. Table 2 gives values of α and β at $Re=4500$ for *Grid 4*, and the above discussions imply that the stability of the present method depends only on the Courant number α; it is stable when $\alpha<1$, a reasonable result for the implicit method. Even for a fairly large $\Delta\tau=0.02$, the appearance of instability is delayed quite a lot; the procedure appears to be stable up to about 250 time-steps, but then it blows up in just a few time-steps. This is because, just after the start of motion, the vorticity is clustered near the surface where the local Courant number is less than one owing to

Table 2 Parameters α and β at $Re=4500$ for *Grid 4*

$\Delta\tau$	α	β
10^{-5}	9.1×10^{-4}	0.0556
2×10^{-4}	0.0182	1.11
5×10^{-4}	0.0455	2.78
0.001	0.091	5.56
0.01	0.91	55.6
0.02	1.82	111.1

the low velocity; only after the vorticity diffuses deep into the fluid where the local Courant number is greater than one, will instability appear.

Values of transient drag coefficients at $\tau=0.1$ and nearly steady ones at $\tau=500.1$ for a circular cylinder at $Re=4500$, computed varying the time-step $\Delta\tau$, are in Table 3[2] and relative errors $(C_D-C_{D0})/C_{D0}$ in Fig. 6, where C_{D0}'s are the estimated values of drag coefficients for $\Delta\tau=0$. For C_D's at $\tau=500.1$, we did not compute the flow field with small time-steps from the start, but with a fairly large time-step $\Delta\tau=0.001$ up to $\tau=500$ and then switched to smaller time-steps. The figure shows that the method has the global accuracy of first order.

It is interesting that the nearly steady solution at $\tau=500.1$ still depends on the magnitude of $\Delta\tau$.

Table 3 Computed drag coefficients of a circular cylinder ($Re=4500$, *Grid 4*)

$\Delta\tau\times10^5$	$\tau=0.1$		$\tau=500.1$	
	C_D	$\Delta C_D\times10^5$	C_D	$\Delta C_D\times10^5$
1	0.70241	1	0.75643	4
2	0.70242	2	0.75640	1
5	0.70246	6	0.75643	4
10	0.70253	13	0.75647	8
20	0.70266	26	0.75656	17
50	0.70306	66	0.75682	43
100	0.70373	133	0.75725	86
0	0.70240		0.75639	

1. The values of C_{D0} at $\Delta\tau=0$ are estimated ones.
2. $\Delta C_D=C_D-C_{D0}$

2) The value of about 0.76 for the drag coefficient of a circular cylinder is rather small compared to the commonly accepted experimental value of about 1.2. This seems due to the annihilation of the vortex street as the result of the forced symmetric flow. Roshko(1954), for example, shows that the drag coefficient of a circular cylinder at $Re=7250$ is reduced to about 0.72, if the splitter plate of length $10a$ is attached at the rear of the cylinder.

But the "steady" solution we are talking about here does not mean the solution of the steady algebraic equations, that is, the solution of Eqs. (30) to (35) with the left-hand side of Eq. (32) replaced by zero, but the stationary solution of the approximate procedure, where the internal vorticities are obtained first replacing Eq. (35) by Eq. (36) and then vorticities at the solid boundary are adjusted using Eq. (35). Physically, this means that the vorticity in the region decreases continuously throughout the interval $\Delta\tau$ and then is recharged just at the end of the interval. In a steady flow, the amount of vorticity convected out through the outflow boundary during the interval Δt will be the same as that flowing into the fluid from the solid surface and thus equal to

$$\left(-\int_0^{s_L}\nu\frac{\partial\omega}{\partial n}ds\right)\Delta t = \left(\int_0^{s_L}\frac{1}{\rho}\frac{\partial p}{\partial s}ds\right)\Delta t=-\frac{p_0-p_b}{\rho}\Delta t, \quad (46)$$

where s, n are coordinates along and normal to the surface, ρ, μ the density and viscosity of the fluid, and p_0, p_b the pressure at the front and rear stagnation point, respectively, and s_L is the distance from the front stagnation point to the rear one. In the numerical procedure considered here, this loss of vorticity will be recharged at the end of the interval Δt in the cells adjacent to the wall,

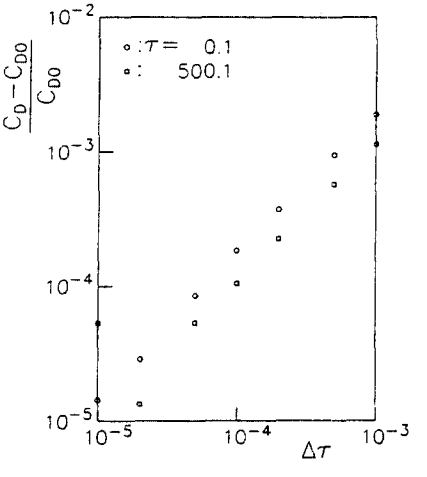

Fig. 6 Relative error in drag coefficients of an impulsively started circular cylinder versus time-step size ($Re=4500$, *Grid 4*)

and the vorticity at the wall will be added by the amount, in average,

$$\Delta\omega \approx -\frac{(p_0-p_b)\Delta t}{\rho s_L \Delta n_{min}},$$

or

$$\frac{-\mu\Delta\omega}{p_0-p_b} \approx \frac{\nu\Delta t}{s_L\Delta n_{min}} \sim \frac{\Delta\tau}{Re\Delta\psi_{min}}.$$

Thus we have

$$\frac{\Delta C_D}{C_{D0}} \equiv \frac{C_D-C_{D0}}{C_{D0}} \sim \frac{\Delta\tau}{Re\Delta\psi_{min}}. \quad (47)$$

Figure 7 shows that the above relation holds quite well over a fairly wide range of $\Delta\tau$ and Re. In fact, ΔC_D is a little different from an error in the ordinary sense. ΔC_D itself is nearly proportional to $\Delta\tau$ and C_{D0} can be estimated fairly accurately; scattering at small $\Delta\tau$ is thought largely due to single-precision(32-bit) arithmatic.

The flow around an impulsively started sphere at $Re=10$ has also been solved to check the validity of the computer code to an axi-symmetric flow. Figure 8 shows the computational grid used to compute the flow around the sphere, which is quite similar to that for the circular cylinder. In Fig. 9, the computed drag coefficients of the sphere at $Re=10$ are compared with the analytical result (Koh, 1993b).

$$ReC_D = \frac{12}{\sqrt{\pi}}\left(\frac{Re}{\tau}\right)^{0.5}, \quad \tau/Re \ll 1. \quad (48)$$

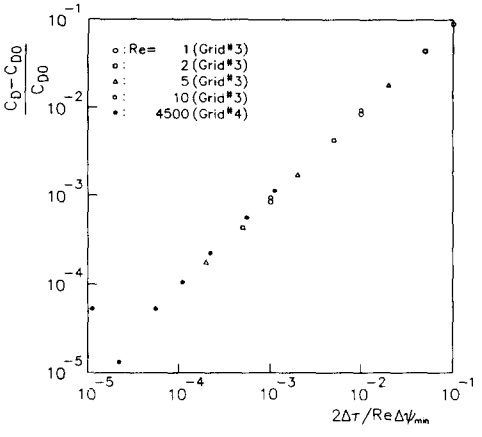

Fig. 7 Relative error in steady-state drag coefficients of a circular cylinder versus time-step size computed using *Grid 3* and *4*

Again the agreement between computed values and analytic ones is quite good at small time.

To solve the system of algebraic equations for both the velocity and vorticity, we have used the point successive-over-relaxation method. The relaxation factors used for the vorticity equation are rather small, usually around 1.1, and go up to about 1.5 only when $\Delta\tau$ is extremely large, and it needs only about 10 to 20 iterations to reduce the relative error to 10^{-6}. On the other hand, the optimum relaxation factors for the velocity are fairly large ranging from about 1.9 to 1.95, which means that the convergence will be rather slow; it requires about 150 to 200 relaxations for the relative error to go down to 10^{-5}. All the computations were carried out using personal computers and work-stations. In IBM386DX, as an example, about 100 time-steps can be executed in an hour when *Grid 3* (70×35 meshes) is employed, while HP720 work-station can do about 600 time-step calculations per hour with *Grid 4* (90×50 meshes).

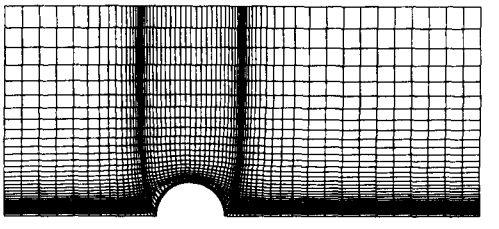

Fig. 8 Computational grid for a sphere

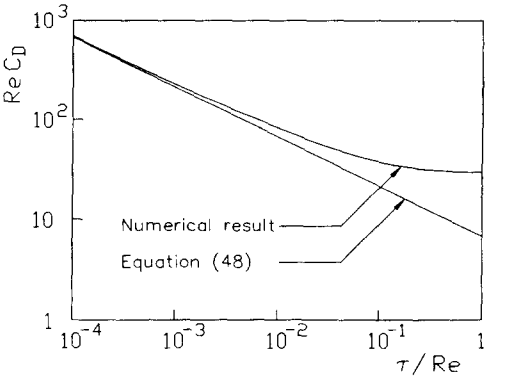

Fig. 9 Drag coefficient of an impulsively started sphere at $Re=10$

5. Conclusions

A numerical method to solve two-dimensional and axi-symmetric incompressible flow has been developed. The present method employs the vorticity-velocity formulation and uses the equipotential lines and streamlines of an inviscid flow as coordinate lines. Velocities are computed directly from the definition of vorticity and continuity equation, with boundary conditions for the normal velocity only, while conditions on the tangential velocity at the boundary are used as boundary conditions for the vorticity.

The accuracy, stability, and other characteristics of the numerical method have been discussed based on the results of numerical simulation of the unsteady flow around an impulsively started circular cylinder and sphere. These numerical experiments confirm that the method is very stable and accurate.

Acknowledgements

It is acknowleged that the present research was supported by the Korean Science Foundation under contract No. 901-0902-027-2. We also appreciate helpful comments and suggestions of Prof. Milovan Peric in the course of preparing the manuscript.

References

Bontoux, P., Smutek, C., Roux, B. and Lacroix, J. M., 1986, "Three-Dimensional Buoyancy-Driven Flows in Cylindrical Cavities with Differentially Heated Endwalls. Part 1. Horizontal Cylinders," J. Fluid Mech., Vol. 169, p. 211.

Campion-Renson, A. and Crochet, M. J., 1978, "On the Stream Function-Vorticity Finite Element Solutions of Navier-Stokes Equations," Int. J. Numer. Methods Eng., Vol. 12, p. 1809.

Chorin, A. J., 1968, "Numerical Solution of the Navier-Stokes Equations," Math. Comput, Vol. 22, p. 745.

Dennis, S. C. R., Ingham, D. B. and Cook. R. N., 1979, "Finite-Difference Methods for Calculating Steady Incompressible Flows in Three-Dimensions," J. Comput. Phys., Vol. 33, p. 325.

Fasel, M., 1976, "Investigation of the Stability of Boundary Layer by a Finite-Difference Model of the Navier-Stokes Equations," J. Fluid Mech., Vol. 78, p. 355.

Fasel, M. and Booz, O., 1984, "Numerical Investigation of Super-Critical Taylor-Vortex Flow for a wide Gap," J. Fluid Mech., Vol. 138, p. 21.

Fletcher, C. A. J., 1988, *Computational Techniques for Fluid Dynamic 2*, Springer-Verlag, New York/Berlin.

Gatski, T. B., Grosch, C. E. and Rose, M. E., 1982, "A Numerical Study of the Two-Dimensional Equations in Vorticity-Velocity Variables," J. Comput. Phys., Vol. 48, p. 1.

Gatski, T. B., Grosch, C. E. and Rose, M. E., 1989, "The Numerical Solution of the Navier-Stokes Equations for 3-Dimensional, Unsteady, Incompressible Flows by Compact Schemes," J. Comput. Phys., Vol. 82, p. 298.

Harlow, F. H. and Welch, J. E., 1965, "Numerical Calculation of Time-Dependent Viscous Incompressible Flow," Phys. Fluids, Vol. 8, p. 2182.

Jordan, S. A., 1992, "An Iterative Scheme for Numerical Solution of Steady Incompressible Viscous Flows," Computers Fluids, Vol. 21, p. 503.

Koh, Y. -M., 1987, *Numerical Solution of Three-Dimensional Vorticity Transport Equations*, Ph. D. Thesis, Dept. of Aeronautics, Imperial College, Univ. of London.

Koh, Y.-M., 1993a, "Pressure Distribution and Flow Development in Unsteady Incompressible Laminar Boundary Layers," KSME J., Vol. 7, p. 213.

Koh, Y. -M., 1993b, "The Pressure Distribution around Unsteady Boundary Layers," J. Fluid Mech., Vol. 255, p. 437.

Lamb, H., 1945, *Hydrodynamics*, 6th ed., Dover, New York.

Lighthill, M. J., 1963, "Introduction. Boundary Layer Theory," Ch. II of *Laminar Boundary Layers*, ed. by L. Rosenhead, Clarendon Press, Oxford.

Patankar, S. V. and Spalding, D. B., 1972, "A Calculation Procedure for Heat, Mass, and Momentum Transfer in Three-Dimensional Parabolic Flows," Int. J. Heat Mass Transfer, Vol. 15, p. 1787.

Roshko, A., 1954, "On the Drag and Shedding Frequency of Two-Dimensional Bluff Bodies," NACA TN 3169.

Rubin, S. G. and Khosla, P. K., 1981, "Navier-Stokes Calculations with a Coupled Strongly Implicit Method — I. Finite-Difference Solution," Computers Fluids, Vol. 9, p. 163.

Truesdell, C., 1954, *The Kinematics of Vorticity*, Indiana Univ. Press, Bloomington.